# Adiabatically controlled motional states of a $CaO^+$ and $Ca^+$ trapped-ion chain cooled to the ground state

Lu Qi (亓鲁),[1,2,*] Evan C. Reed,[1,2] and Kenneth R. Brown[1,2,3,†]
[1]*Duke Quantum Center, Duke University, Durham, North Carolina 27701, USA*
[2]*Department of Electrical and Computer Engineering, Duke University, Durham, North Carolina 27708, USA*
[3]*Departments of Physics and Chemistry, Duke University, Durham, North Carolina 27708, USA*

(Received 21 December 2022; revised 24 April 2023; accepted 22 June 2023; published 13 July 2023)

Control of the external degree of freedom of trapped molecular ions is essential for their promising applications to spectroscopy, precision measurements of fundamental constants, and quantum information technology. Here, we demonstrate near ground-state cooling of the axial motional modes of a calcium mono-oxide ion via sympathetic sideband cooling with a cotrapped calcium ion. We also show that the phonon state of the axial out-of-phase mode of the ion chain is maintained while the mode frequency is adiabatically ramped up and/or down. The adiabatic ramping of the motional mode frequency is a prerequisite for searching for the proposed molecular dipole-phonon interaction [W. C. Campbell and E. R. Hudson, Phys. Rev. Lett. **125**, 120501 (2020); M. Mills *et al.*, Phys. Chem. Chem. Phys. **22**, 24964 (2020)].

DOI: 10.1103/PhysRevA.108.013108

## I. INTRODUCTION

Molecular ions are promising candidates for precision spectroscopic measurements, such as determination of molecular properties [1,2], searching for the possible time variations of the electron-to-proton mass ratio [3–7], and determination of the electron electric dipole moment [8–10]. For these experiments, it is a prerequisite that the motional energy of molecular ions is reduced to eliminate systematic effects such as Doppler shifts. Molecular ions can be translationally cooled through Doppler cooling cotrapped atomic ions with benefits for spectroscopy and understanding chemical reactions [11–13]. In quantum logic spectroscopy experiments in which molecular ions' internal states are mapped to their motional states, the molecular ions need to be further cooled to near the ground state of motion [14–19] for higher signal-to-noise ratio. This motional ground state cooling is achieved via sympathetic resolved sideband cooling with cotrapped atomic ions [20].

Recently, a quantum logic scheme based on the interaction of the permanent electric dipole of trapped diatomic molecular ions and their quantized harmonic motion known as dipole-phonon quantum logic (DPQL) has been proposed [21]. In Ref. [22], a list of cationic alkaline-earth-metal monoxides and monosulfides, which can be produced from commonly trapped atomic ions, were studied as potential candidates for DPQL. From this list of molecular ions, calcium monoxide ($^{40}Ca\,^{16}O^+$) is a promising candidate, because the Λ-doublet transition frequencies of its low-lying rotational states are calculated to be within the range of typical ion trap secular frequencies [14,22,23]. Note that from here on the same isotopes of calcium and oxygen are used unless otherwise specified. One way to implement DPQL with a $Ca^+$-$CaO^+$ ion chain is to slowly ramp the motional mode frequency through a resonance with $CaO^+$'s Λ-doublet splitting to achieve adiabatic passage between the two dressed states of Λ-doublet states and phonon states. At the end of this process, the Λ-doublet state change of $CaO^+$ is mapped to its motional state, and either a phonon appears in the system, indicating a change from the upper to the lower Λ-doublet state, or a phonon disappears, indicating the reverse process. The motional state change is read-out via a red sideband operation on the cotrapped $Ca^+$. During this process, cooling the ion chain to near the motional ground state is an advantage, as the detection can become single shot, similar to quantum logic schemes [14–18]. The ramping process, on one hand, has to be fast to prevent motional heating from deteriorating the signal-to-noise ratio. On the other hand, the ramping process needs to be slow to meet the requirement for adiabaticity and ensure that the motional state change is due to the dipole-phonon interaction instead of a diabatic perturbation of the motional state [22]. Beyond direct applications to DPQL, adiabatic motional dynamics in ion shuttling and separating has been studied both theoretically [24,25] and experimentally [26–28], and adiabatic motional frequency ramping has been demonstrated with single $Ca^+$ [29,30] and $^{40}Ca^+$-$^{42}Ca^+$ ion chain [30].

In this paper, we demonstrate near-ground-state cooling of both the axial in-phase and out-of-phase motional modes of a $Ca^+$-$CaO^+$ ion chain. We also demonstrate the ability to adiabatically ramp the out-of-phase mode frequency over the calculated Λ-doublet splitting of the ground rotational state of $CaO^+$ while maintaining the phonon state of the ion chain. While we have not made a significant effort to observe the dipole-phonon interaction thus far, this work demonstrates the external state control and preparation necessary to search for the dipole-phonon interaction with $CaO^+$. Besides the

*lu.qi@duke.edu
†kenneth.r.brown@duke.edu

 

application to DPQL, this technique may also benefit quantum logic spectroscopy of molecular ions [29,30] by controlling the zero-point fluctuations in momentum or benefit ultracold ion chemistry [31] by further controlling collisions [32]. This paper is arranged as follows. In Sec. II, we analyze the heating mechanisms that may occur during adiabatic ramping. In Sec. III, we introduce our experimental system and sideband cooling techniques. In Sec. IV, we discuss the results of ground-state cooling and adiabatic ramping before summarizing in Sec. V.

## II. HEATING MECHANISM ANALYSIS IN ADIABATIC RAMPING

Implementation of DPQL depends on precise measurement of the number of phonons. The key systematic error that interferes with the measurement is motional heating. Moreover, motional heating limits the fidelity of the dipole-phonon interaction [22]. In this section, we analyze two potential ion heating mechanisms and determine the sufficient experimental parameters to measure DPQL.

### A. Axial motional mode heating rate analysis

The heating rate of the motional mode needs to be low enough to support a clean signal-to-noise ratio for the DPQL signal. The pseudopotential experienced by a single $Ca^+$ ion in an RF trap is of the form: $U(x,y,z) = \frac{1}{2}m\omega_x^2x^2 + \frac{1}{2}m\omega_y^2y^2 + \frac{1}{2}m\omega_z^2z^2$, where $m$ is the mass of $Ca^+$, $\omega_x$ and $\omega_y$ are radial secular frequencies, and $\omega_z$ is the axial secular frequency. Now consider a two-ion chain of $Ca^+$-$CaO^+$ in the above potential. The two ions are located equidistantly from the center of the trap by a distance of $d_0 = \sqrt[3]{e^2/16\pi\epsilon_0 m\omega_z^2}$ along the axial direction due to Coulomb interaction, where $e$ is the element charge and $\epsilon_0$ is the vacuum permittivity. Around the equilibrium positions, two ions behave as coupled harmonic oscillators, which results in two normal motional modes: the in-phase mode ($i$), where the two ions move in the same direction, and the out-of-phase ($o$) mode, where the two ions move in opposite directions. The two motional mode frequencies, $\omega_i$ and $\omega_o$, are calculated as [33]

$$\omega_{i,o} = \sqrt{\frac{1+\mu \mp \sqrt{1-\mu+\mu^2}}{\mu}}\omega_z, \tag{1}$$

where $\mu = 1.4$ is the mass ratio of $CaO^+$ to $Ca^+$ and the minus and the plus in the equation correspond to the in-phase mode and out-of-phase mode, respectively.

Here, we consider typical motional heating mechanisms in ion traps, which are spatially uniform, stochastic electrical fields from fluctuating patch-potentials and thermal electronic noise [34]. The corresponding heating rates $\Gamma_{i,o}^{0\to1}$ from the ground state ($|n=0\rangle$) to the first excited state ($|n=1\rangle$) for both $i$ and $o$ axial modes are [20]

$$\Gamma_{i,o}^{0\to1} = \frac{e^2S_E(\omega_{i,o})}{4m\hbar\omega_{i,o}}\left(b_{i,o} + \sqrt{\frac{1-b_{i,o}^2}{\mu}}\right)^2. \tag{2}$$

Here, $S_E(\omega)$ is the spectral density of electric field fluctuations in the unit of $(V/cm)^2\ Hz^{-1}$, and $b_{i,o}$ are the components of the normalized eigenvectors of the normal motional modes of $Ca^+$ with $b_i = 0.58$ and $b_o = -0.81$. Assuming a white noise spectrum around the trap frequency, we can normalize Eq. (2) with the single $Ca^+$ heating rate $\Gamma_{Ca}^{0\to1} = e^2S_E(\omega_z)/4m\hbar\omega_z$ of the same electric potential and calculate the following ratios:

$$\Gamma_i^{0\to1} = 1.78\Gamma_{Ca}^{0\to1}, \tag{3a}$$

$$\Gamma_o^{0\to1} = 0.06\Gamma_{Ca}^{0\to1}. \tag{3b}$$

This indicates that the out-of-phase motion of the two ions is hardly heated by this heating mechanism compared to the in-phase motion, since the anticorrelated motion of the out-of-phase mode is unperturbed in the spatial uniform electrical fields. Based on the above analysis, the out-of-phase mode has the advantage of a lower heating rate compared to the in-phase mode and thus is used for adiabatic ramping in the following experiments.

### B. Phonon-phonon interaction from radial modes

Another heating mechanism that needs to be avoided is the phonon-phonon interaction between the axial mode and radial modes, since the uncooled radial modes act as a hot bath during the adiabatic ramping process. We consider two cases of this interaction here. One is due to imperfect micromotion compensation. In a linear Paul trap, ions are trapped in the pseudopotential $\phi(r_i = x, y)$ along the radial directions $x$ and $y$:

$$\phi_i \approx \frac{(eV_0)^2}{4m_iR^4\omega_{rf}^2}r_i^2. \tag{4}$$

Here, $V_0$ and $\omega_{rf}$ are the radio-frequency (rf) voltage and frequency, $m_i$ is the mass of the $i$th ion, and $R$ is the distance from the ion to the rf electrodes. We ignore radial potential changes from axial end-caps as they are small compared to the radial pseudopotential. As Eq. (4) shows, ions of different masses see different radial potential depths in a mixed-species ion chain. As a result, this ion chain is no longer along the trap axis if there are any residual stray electric fields along the radial direction, since each ion is displaced from the rf null as a function of mass [23]. Consider a two-ion chain of $Ca^+$-$CaO^+$. Suppose a residual stray field along the $x$ axis and the angle between the interion axis and the trap axis is $\theta \ll 1$. The position difference along the $x$ axis $\Delta x \equiv |x_{CaO} - x_{Ca}|$ is no longer 0 but $r\theta$, where $r$ is the interion distance. In this situation, the axial and radial cross terms appear in the potential as $|\frac{\partial^2V}{\partial x_i\partial z_j}| = \frac{3m\omega_z^2}{2}\theta q_{ix}q_{jz}$. Here, $q_{ix}$ and $q_{jz}$ are the $x$ and $z$ position operators for the harmonic motions of $Ca^+(i,j=1)$ and $CaO^+(i,j=2)$. The corresponding perturbation Hamiltonian $\Delta H_1$ is

$$\Delta H_1 = \sum_{i,j=1}^{2}(-1)^{(i-j)}3m\omega_z^2\theta q_{ix}q_{jz}. \tag{5}$$

Phonon-phonon interaction between radial and axial motion happens when the radial mode frequency is in resonance with the axial mode frequency in the presence of an uncompensated radial stray field as shown in Eq. (5). When the frequencies of axial and radial out-of-phase modes overlap, the phonon exchange rate could be as high as 1% of $\omega_z$ even with $\theta$ as

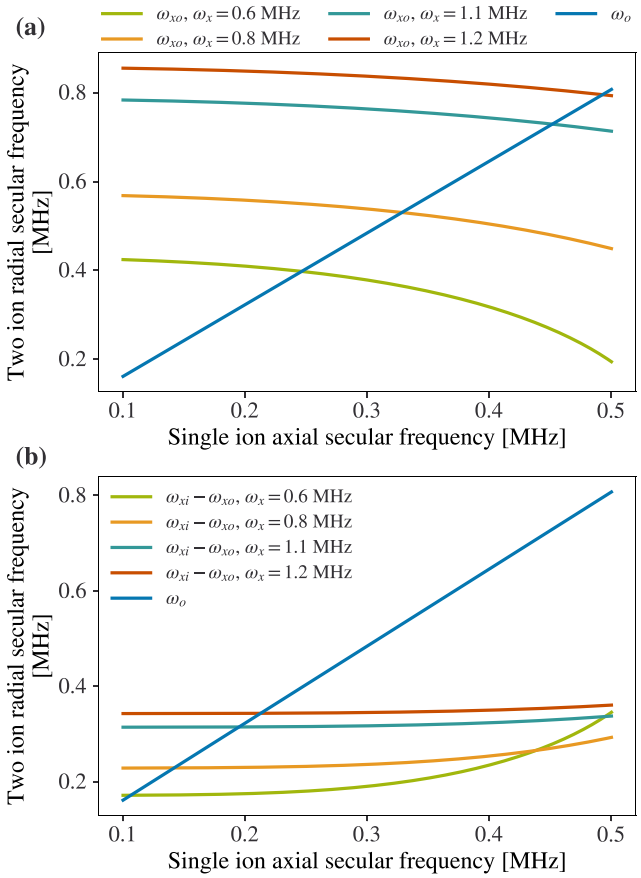


FIG. 1. $Ca^+$-$CaO^+$ ion chain mode frequencies with respect to single $Ca^+$ mode frequencies. (a) $Ca^+$-$CaO^+$ ion chain axial out-of-phase mode frequency $\omega_o$ and radial out-of-phase mode frequency $\omega_{xo}$ with respect to single $Ca^+$ axial mode frequency under radial potentials $\omega_x = 1.2$, 1.1, 0.8, and 0.6 MHz [for horizontal lines from top to bottom, same as in panel (b)]. (b) $Ca^+$-$CaO^+$ ion chain frequency differences between radial in-phase mode $\omega_{xi}$ and out-of-phase mode $\omega_{xo}$, and axial out-of-phase mode frequency $\omega_o$ with respect to single $Ca^+$ axial mode frequency under different radial potentials $\omega_x$. Each of the crossing points between $\omega_o$ and $\omega_{xo}$ or $\omega_{xi}$-$\omega_{xo}$ represents phonon-phonon interaction occurrences, which need to be avoided in the adiabatic ramping experiments.

low as 0.01. In Fig. 1(a), we plot both the radial and the axial out-of-phase mode frequencies $\omega_{xo}$ and $\omega_o$ of a $Ca^+$-$CaO^+$ ion chain with respect to the single $Ca^+$ ion axial secular frequency $\omega_z$ under different radial secular frequencies $\omega_x$. In our experiment, the radial secular frequency is carefully chosen to avoid the frequency overlapping point as shown in Fig. 1, so that the axial out-of-phase mode is isolated from the radial modes during the ramping process.

Another phonon-phonon coupling mechanism comes from the anharmonicity caused by Coulomb interaction between ions [35]. Performing a Taylor expansion to the third order of the potential $V$ of the $Ca^+$-$CaO^+$ ion chain around the equilibrium positions, we can get the anharmonicity Hamiltonian $\Delta H_2$ as a perturbation to the harmonic potential:

$$\Delta H_2 = -\frac{1}{6}\sum_{m,n,p=1}^{2}\sum_{i,j,k=1}^{3}\frac{\partial^3 V}{\partial r_{mi}\partial r_{nj}\partial r_{pk}}\bigg|_0 q_{mi}q_{nj}q_{pk}, \qquad (6)$$

where $r_m$ is the position of the $m$th ion and $r_{mi} = (x_m, y_m, z_m)$ with $i = 1$, 2, and 3. This shows that energy can be transferred once the frequency sum or difference of two modes is near resonant with another mode frequency. Equation (6) can be simplified to Eq. (7) based on the fact that $Ca^+$ primarily participates in the radial in-phase mode while $CaO^+$ primarily participates in the radial out-of-phase mode:

$$\Delta H_2 = \sum_{i=1}^{2}\frac{3m\omega_z^2}{4z_0}q_{1i}q_{2i}(q_{23} - q_{13}). \qquad (7)$$

The above equation shows that phonon-phonon interaction happens once the frequency difference between radial in-phase and radial out-of-phase modes is in resonance with the axial out-of-phase mode frequency. We plot the axial out-of-phase mode frequency and the radial frequency difference with respect to the single $Ca^+$ axial secular frequency $\omega_z$ and a set of various single-ion radial secular frequencies $\omega_x$ in Fig. 1(b). The coupling strength is $2\pi \times 8.2$ Hz for an out-of-phase mode frequency around $2\pi \times 320$ kHz and $\omega_x = 1.1$ MHz in Fig. 1(b). Similarly to the consequence of the findings from Fig. 1(a), the radial secular frequency is chosen to avoid crossing points on the axial out-of-phase mode of Fig. 1(b).

### C. Ramping parameter analysis

A simple model for the adiabatic passage under the dipole-phonon coupling is obtained using a dressed state picture: $|+\rangle = |f, n_q\rangle$ and $|-\rangle = |e, n_q + 1\rangle$, where $|f\rangle$ and $|e\rangle$ are the upper and lower $\Lambda$-doublet states, respectfully, and $n_q$ is the phonon number of the motional mode $q$. In this picture, an avoided crossing between $|+\rangle$ and $|-\rangle$ is formed when $\omega(t)$ is near resonance with the resonant frequency of the $\Lambda$-doublet splitting, denoted as $\omega_{\rm mol}$. The energy gap of the avoided crossing is $\Delta E(t) = \hbar\sqrt{g_{\rm mol}^2 + (\omega(t) - \omega_{\rm mol})^2}$, where $\omega(t)$ is the time-varying phonon mode frequency, $g_{\rm mol} \equiv d\mathcal{E}_0 = \frac{d}{e}\sqrt{2\mu m\omega_o^3/\hbar}\sqrt{1 - b_o^2}$ is the vacuum Rabi frequency of the interaction, $\mathcal{E}_0$ is the electric field amplitude at the position of $CaO^+$ due to a single phonon in the out-of-phase mode, $d = \Omega/\sqrt{J(J+1)}D_P$ is the dipole moment of the $\Lambda$-doublet transition, $\Omega$ is the projection of the total electronic angular momentum along the internuclear axis, $J$ is the total angular momentum, and $D_P$ is the permanent dipole moment. The narrowest part of this energy gap, $\Delta E_{\rm min} = \hbar g_{\rm mol}$, sets the limit for the ramping speed $d\omega(t)/dt$. For a high-fidelity transfer, $d\omega(t)/dt \ll g_{\rm mol}^2$ must be satisfied [36]. For the ground rotational state of $CaO^+$, $\Omega = J = 3/2$ and $D_P$ is 8.7 Debye [22]. In a $Ca^+$-$CaO^+$ ion chain, $g_{\rm mol} = 2\pi \times 2.6$ kHz for the ground rotational state of $CaO^+$ in the out-of-phase mode. Thus, the ramping speed should be less than $2\pi \times 42.5$ kHz/ms. Given that the starting and ending points for the frequency sweep are chosen to be 10 $g_{\rm mol}$ from the resonance $\omega_{\rm mol}$ in order to minimize coupling between the $\Lambda$-doublet and the phonon state, a total ramping time of several milliseconds is needed.

Since the dipole-phonon coupling puts a much more stringent limit on the ramping speed [22], the diabatic motional state excitation is negligible during the ramping process. Thus, a simple linear voltage ramping for the end-cap voltages ($V_{\rm end}$)

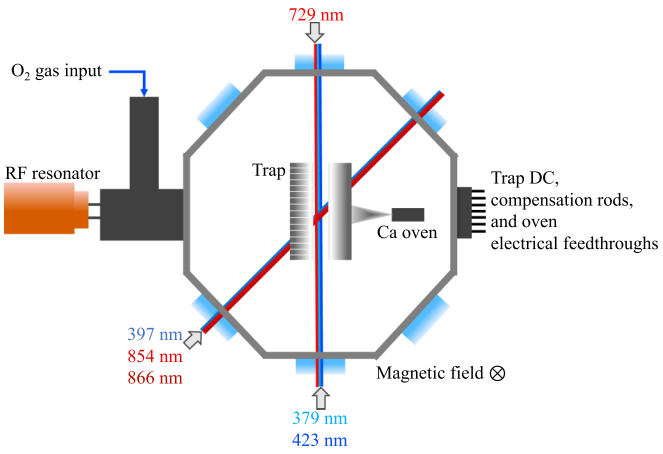


FIG. 2. Schematic of the experimental system. The magnetic field is aligned in the vertical direction and is perpendicular to the polarization of the 729-nm laser. The imaging lens stack (not shown) is also aligned in the vertical direction outside the vacuum chamber with its center positioned directly above the ions.

is used. Despite $\omega(t) \propto \sqrt{V_{\text{end}}}$, the linear voltage ramping shape results in an almost linear secular frequency ramping shape, since the ramping range (20 $g_{\text{mol}}$) is much less than the secular frequency itself (∼200 $g_{\text{mol}}$). The other limit on ramping time is the heating rate of the system, as the motional heating decreases the signal-to-noise ratio for long ramping time. To avoid this, the ramping time could be further reduced in a nonlinear ramping process, as studied in Refs. [30,37].

## III. EXPERIMENTAL METHODS

### A. Experimental system

A schematic of our experiment system is shown in Fig. 2. Our linear Paul trap [14,23] sits in an ultrahigh vacuum, octagonal chamber (Kimball Physics MCF800-SphOct-G2C8) with a typical pressure of $2 \times 10^{-11}$ Torr. The radial potential is created by four wedge-shaped electrodes, two rf electrodes ($x$ axis), and two segmented dc electrodes ($y$ axis). The distance from the ions to the electrodes is $r_0 = 1.0$ mm. The rf electrodes are driven by a helical resonator with a frequency of $2\pi \times 19.2$ MHz. There are two rods, one above and one below the trap, that are parallel to the trap axis to provide micromotion compensation. The trap has typical secular frequencies of $(\omega_x, \omega_y, \omega_z)/2\pi = (1.12, 1.08, 0.45)$ MHz for a single $Ca^+$ ion. A magnetic field of 6.2 G generated by permanent magnets is applied to lift the degeneracy of Zeeman states and defines the quantization axis along the vertical direction. A lens stack (not shown) is set up above the trap to collect fluorescence for a photomultiplier tube (Hamamatsu H7360-02) and a high-sensitivity camera (Princeton Instruments Cascade 1K).

The voltage control of dc electrodes and two micromotion compensation rods is achieved using a 16-bit digital analog converter (DAC) board (M-Labs Zotino) with an output cutoff frequency of $2\pi \times 75$ kHz. The DAC outputs are amplified by a factor of 11 using operational amplifiers (LTC6090) and then passed through RLC passive low-pass filters before being applied to the electrodes and rods. The cutoff frequency of the filters is $2\pi \times 1.5$ kHz, which is chosen to filter out ambient electromagnetic noise and rf pickup around the secular frequencies while passing the ramping of the dc voltages on the trap electrodes and compensation rods.

The DAC sequence is controlled by a Kasli FPGA module and programed using ARTIQ (Advanced Real-Time Infrastructure for Quantum physics) provided by M-labs [38,39] using tools developed as part of the Duke ARTIQ extensions (DAX) [40,41]. Each ramping sequence step contains voltages for two pairs of end-cap electrodes and two micromotion compensation rods. The end-cap voltage sequence is designed for a linear sweep, while the micromotion compensation voltages are generated via an interpolation of optimized micromotion compensation voltages for different end-cap voltage setups. The synchronized DAC outputs have a refresh time of 4.8 μs, which is the limiting factor on the discretization of the ramping sequence. The designed ramping sequence is preloaded into the system memory and can be played back on demand during the experiment.

$Ca^+$ ions in the trap come from photoionization of the neutral Ca atom beam, which is generated by a heated Ca oven near the trap. The photoionization process is implemented by a combination of 423- and 379-nm lasers. $Ca^+$ ions are then Doppler cooled by a 397-nm laser and an 866-nm laser at an angle of 45° to the $z$ axis. A 729-nm laser with horizontal polarization along the $z$ axis is used to address the quadruple transition $|S_{1/2}, m_S = -1/2\rangle \rightarrow |D_{5/2}, m_D = -5/2\rangle$ for sideband operations. The 729-nm light is from an injection-locked laser diode (HL7301MG-A). The seed laser for injection locking is locked to a high-finesse low-thermal-expansion cavity via the Pound-Drever-Hall method, and the transmitted light of the cavity is used for injection locking. An 854-nm laser is used to pump $Ca^+$ ions from the $D_{5/2}$ manifold to quench the excited state and accelerate sideband operations.

$CaO^+$ ions are synthesized by introducing $O_2$ into the chamber. To begin, two $Ca^+$ ions are trapped and cooled in the ion trap. Then, $O_2$ is leaked into the chamber via a manual leak valve. The vacuum pressure is kept around $5 \times 10^{-9}$ Torr until one of the $Ca^+$ ions reacts to form $CaO^+$ and becomes a dark ion in the trap. Since, for the electronic state of $Ca^+$ ($^2S_{1/2}$), this reaction is endothermic by 1.7 eV, it presumably proceeds as $Ca^+(^2P_{1/2}) + O_2 \rightarrow CaO^+ + O$. In our system, $CaO^+$ stays for about 20 min before it reacts with background gas and turns into $CaOH^+$. We confirm whether the dark ion is $CaO^+$ or $CaOH^+$ by measuring the axial secular frequency [42] to a precision of 1 kHz by resonant excitation with an oscillating electric field.

### B. Pulsed sideband cooling

Pulsed sideband cooling is used in our experiments to cool either a single ion or a two-ion chain to motional ground states [30]. In this technique, the 729- and 854-nm lasers are turned on and off sequentially so that the transition frequencies are less effected by light shifts induced by the other laser. The pulse sequences are shown in Fig. 3(a). After Doppler cooling, the $Ca^+$ ion is in a thermal state with the average axial phonon number $\bar{n}$ around the Doppler cooling limit $\Gamma_{397}/2\omega_z \approx 25$, where $\Gamma_{397} \approx 2\pi \times 21$ MHz is the natural line width of the $S_{1/2} \leftrightarrow P_{1/2}$ transition. In this thermal state, ∼40% of the

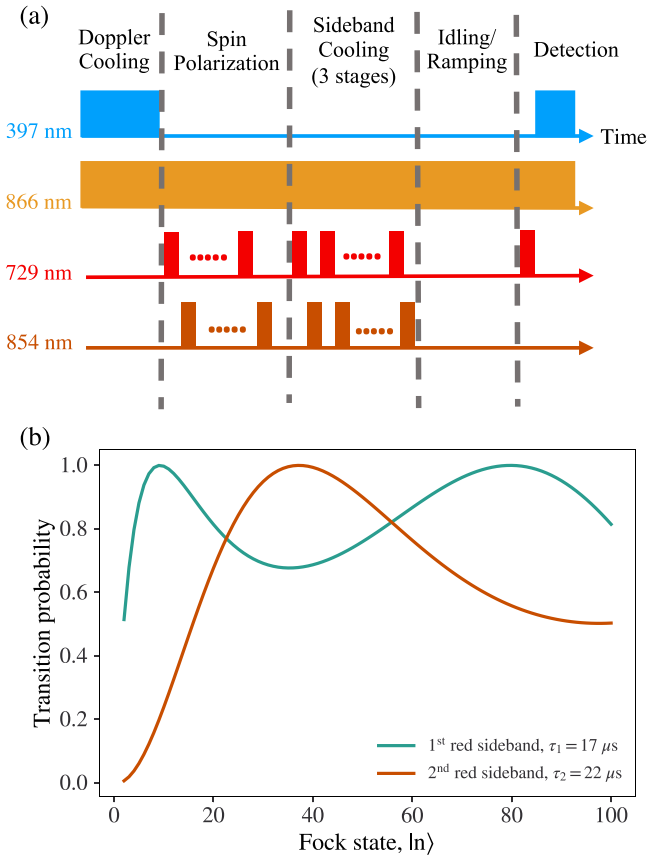


FIG. 3. (a) Experimental sequence. The ions are first Doppler cooled and, subsequently, a multiorder sideband cooling method is employed after spin polarization, as detailed in the text. Depending on the experiment, we either ramp the trap frequency or allow for an idle period before measuring the red sideband via shelving to the $D_{5/2}$ state. (b) Fock-state-dependent transition probability for a single ion for the first-order [green (light gray) line] and second-order [red (dark gray) line] sidebands for a carrier Rabi frequency of $\Omega_0 = 2\pi \times 70$ kHz at times $\tau_1$ and $\tau_2$, respectively.

population is out of the Lamb-Dicke (LD) regime. This highly energetic portion of the motional state satisfies $\eta^2(2n+1) \geqslant 1$, where $\eta \approx 0.15$ is the LD parameter for a single $Ca^+$ ion along the axial direction and $n$ is the Fock state number. To begin ground-state cooling, first a spin-polarization process is performed utilizing the $|S_{1/2}, m_S = 1/2\rangle \rightarrow |D_{5/2}, m_D = -3/2\rangle$ transition to initialize $|S_{1/2}, m_S = -1/2\rangle$. This process is repeated periodically during sideband cooling to reinitialize the ground state and keep the ion inside the cooling loop. Taking advantage of the fact that such a high-$n$ population is sensitive to higher-order sideband transitions, we cool in three stages. The first stage uses second-order sidebands for cooling. The second and third stage use first-order sidebands. The first and second stage contain four repetitions, each of which includes 20-s first-order red sideband pulses and a round of spin polarization. The third stage contains ten pulses and uses half of the 729-nm optical power of the first two stages to avoid off-resonant coupling to the carrier transition. The pulse numbers provide enough redundancy to cool the ion even when the axial secular frequency is halved. The sideband cooling pulse lengths of the three stages are fixed based on

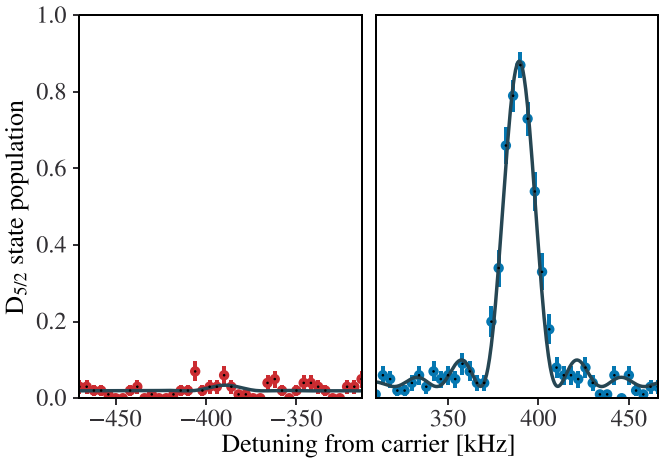


FIG. 4. Sideband measurements after sideband cooling of axial motion of a single $Ca^+$ ion. The plot on the left shows the spectral profile of the first red sideband whereas the right shows the profile of the first blue sideband. Here, the axial secular frequency is $2\pi \times 390$ kHz, which corresponds to an average phonon number of $\bar{n} = 0.06(2)$. The frequency step between each point is $2\pi \times 4$ kHz. Each point is an average of 100 experiments. The solid line is a fit to the sideband data.

expected initial quanta and measured Rabi frequencies. For example, we show in Fig. 3(b) how the first- and second-stage pulse lengths will drive the different initial Fock states for a typical coupling strength (carrier Rabi frequency for $|n = 0\rangle$) of $\Omega_0 = 2\pi \times 70$ kHz. For sideband cooling of the ion chain, similar techniques are used, except that the in-phase and the out-of-phase modes are cooled serially in each stage.

## IV. RESULTS AND DISCUSSION

### A. Sideband cooling of a single $Ca^+$ ion and heating rate measurements

The axial sideband cooling results for a single $Ca^+$ ion with an axial secular frequency of $2\pi \times 390$ kHz are shown in Fig. 4. By comparing the amplitude of the red sideband and the blue sideband, we calculate the average phonon number after sideband cooling to be $\bar{n} = P_r/(P_b - P_r) = 0.06(2)$, where $P_{r/b}$ is the red/blue sideband amplitude. The spectral profile of the red and blue sideband data is fitted via the following model:

$$\rho_{r/b} = \sum_n \frac{\bar{n}^n}{(\bar{n}+1)^{n+1}} \frac{\Omega_{r/b}^2}{\Delta^2 + \Omega_{r/b}^2} \sin^2\left(\sqrt{\Delta^2 + \Omega_{r/b}^2}\, t/2\right), \tag{8}$$

where $n$ is the Fock state number, $\Omega_{r/b}$ is the red/blue sideband Rabi frequency, and $\Delta$ is the detuning. The heating rate measurement results of the axial mode at this frequency are shown in Fig. 5. A heating rate of 11.4(7) $s^{-1}$ is measured at this secular frequency by fitting the average phonon number change with the idling time, In the inset of Fig. 5, heating rate measurements at various axial secular frequencies are shown. The heating rate increases as the secular frequency decreases.

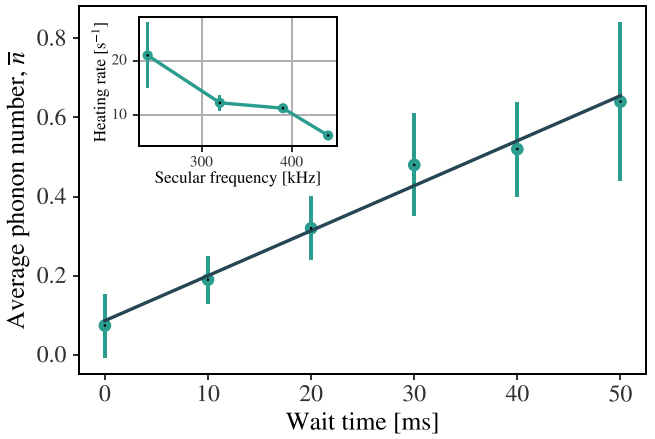


FIG. 5. Average phonon number of a single $Ca^+$ ion as a function of idling time at $\omega_z = 2\pi \times 390$ kHz. A linear fit yields a rate of 11.4(7) s$^{-1}$. The inset shows the heating rate measurements for the axial secular frequency $\omega_z = 2\pi \times 240$, 320, 390, and 440 kHz. The line is to guide the eye.

### B. Sideband cooling of a $Ca^+$-$CaO^+$ ion chain and heating rate measurements

The results of sideband cooling the two axial modes of a $Ca^+$-$CaO^+$ ion chain are shown in Fig. 6. We use the same method as outlined above to determine the average phonon number. We can see that both the in-phase and out-of-phase modes are cooled to near the motional ground state: the in-phase mode is cooled to $\bar{n}_i = 0.12(6)$ and the out-of-phase mode is cooled to $\bar{n}_o = 0.03(1)$.

We also measured the heating rate of both modes and plotted the results as shown in Fig. 7. It was found that the in-phase mode has a heating rate of 23.8(1.5) s$^{-1}$, which is twice the heating rate of a single ion at a similar potential depth. Meanwhile, the out-of-phase mode has a heating rate of 0.5(2) s$^{-1}$, which is 5% of the single-ion heating rate. Comparing the above experimental results with the predictions from Eq. (3), we find the out-of-phase mode heating rate agrees with theoretical prediction. However, the in-phase mode heating rate is ∼20% higher than the theoretical prediction. This is likely due to the less precise determination of phonon numbers above 1 in the heating rate measurement. Because of its low heating rate, the out-of-phase mode is able to support a voltage ramping time on the order of tens of milliseconds without accruing any significant motional heating during the ramping time.

### C. Adiabatic ramping of a $Ca^+$-$CaO^+$ ion chain

We first show how the average phonon number of the out-of-phase mode of the two-ion chain is affected by a linear single-direction ramping sequence. Based on the above analysis of ramping parameters and measured heating rates, we chose the parameters as follows. The ramping range of out-of-phase mode frequency is from $2\pi \times 492$ to $2\pi \times 421$ kHz with a ramping speed of $2\pi \times 10$ kHz/ms. This range covers the predicted Λ-doublet splitting of the ground rotational state of $CaO^+$, which is calculated to be $2\pi \times 450$ kHz. Figures 8(a) and 8(c) show the out-of-phase motional sidebands at the beginning and end of the ramping, respectively.

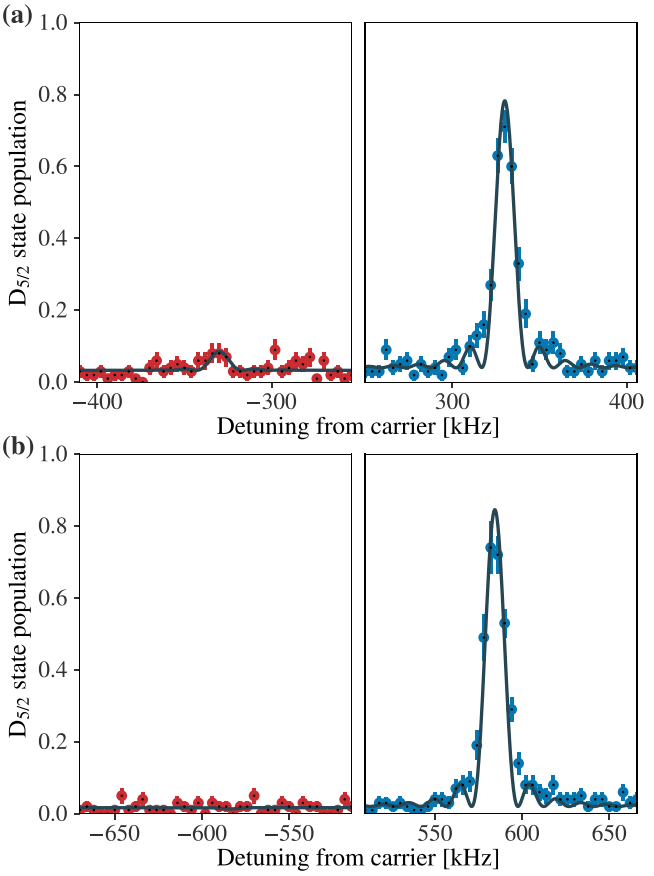


FIG. 6. Sideband measurements after sideband cooling the axial (a) in-phase mode and (b) out-of-phase mode of the $Ca^+$-$CaO^+$ ion chain. Here, the single $Ca^+$ axial secular frequency was set to $\omega_z = 2\pi \times 364$ kHz. The frequency step between each point is $2\pi \times 4$ kHz, and each point is an average of 100 experiments. By comparing the amplitudes, the average phonon number of the in-phase mode after sideband cooling is $\bar{n}_i = 0.12(6)$, while the average phonon number of the out-of-phase mode is $\bar{n}_o = 0.03(1)$.

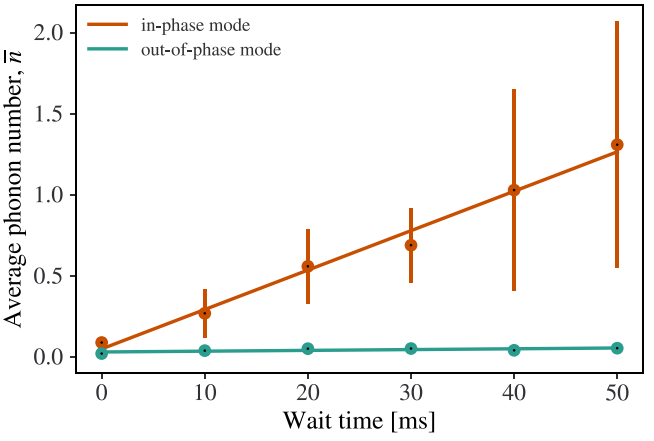


FIG. 7. Heating rate measurements of the axial in-phase (upper line) and out-of-phase (lower line) modes of the $Ca^+$-$CaO^+$ ion chain. Note that the error bars on the out-of-phase data points are not visible because they are smaller than the plotted points.

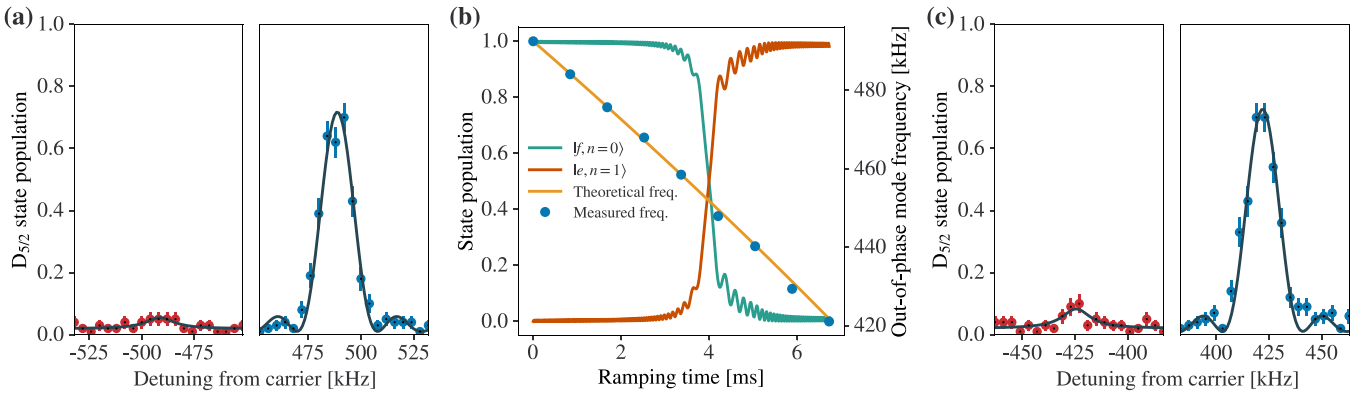


FIG. 8. (a) Out-of-phase motional sidebands after sideband cooling with $\omega_o = 2\pi \times 492$ kHz and $\bar{n}_o = 0.08(2)$. (b) Theoretical secular frequency change during the ramping and measured secular frequency at different points of the ramping. The small difference between theoretical frequency and measured frequency is attributed to environmental magnetic noise. The theoretical ramping sequence is used in a simulation of the dynamics of the dressed states $|f, n = 0\rangle$ (green line, initial state population of 1) and $|e, n = 1\rangle$ (red line, initial state population of 0) with a heating rate of 0.5 $s^{-1}$. In the simulation, the frequency changes with a step of 4.8 μs. (c) Out-of-phase motional sidebands after sideband cooling at $\omega_o = 2\pi \times 492$ kHz and then ramping to $\omega_o = 2\pi \times 421$ kHz using the ramping schedule in panel (b). We find $\bar{n}_o = 0.12(2)$.

The measured phonon number after ramping is $\bar{n}_o = 0.12(3)$ compared to $\bar{n}_o = 0.08(2)$ before ramping. We do not observe a coherent excitation of the ion's motion, which was observed in other adiabatic ramping [30] and ion shuttling experiments [43]. We attribute this to the slow ramping speed and careful alignment of the axial trap position.

In Fig. 8(b), we show the simulation results of the dipole-phonon interaction as the motional mode frequency is swept through resonance with the Λ-doublet. The heating rate in the simulation is set to be 0.5 $s^{-1}$, and the ramping sequence is set to be the theoretical secular frequency change with a refresh time of 4.8 μs. Initial motional state of Fig. 8(a) is measured and used in the simulation. The results show that if the dipole-phonon interaction were to happen in the experiment, it would either add a phonon to the motional mode ($|n = 0\rangle \rightarrow |n = 1\rangle$) or change inversely (if the initial phonon state is prepared in $|n = 1\rangle$). For the former case, the resulting red sideband would have the same height as the blue sideband in Fig. 8(a), and the resulting blue sideband should have a height comparable to that of the resulting red sideband. For the latter case, the resulting red sideband changes inversely and disappears.

In Fig. 9, we compare ramping experiment results with those from experiments in which no ramping was performed. In the latter, the ions were allowed to idle for an amount of time equal to the ramping time. The ramping range of $2\pi \times 200$ kHz, compared to 20 $g_{\mathrm{mol}} \approx 2\pi \times 52$ kHz from the above analysis, leaves space for small calculation inaccuracy or frequency shifts such as Zeeman shifts. We chose a back-and-forth ramping sequence in these results to test whether motional adiabaticity is preserved in both ramping directions. This ramping sequence simplifies phonon-state detection because the secular frequency returns to its initial value after ramping, enabling the 729-nm laser to remain in the same frequency [30,37]. Two total ramping time periods $T_r$, 10 and 20 ms, were chosen for the experiments. Here, it is shown that the out-of-phase mode phonon state is preserved during the ramping process. For $T_r = 10$ ms, the phonon number after

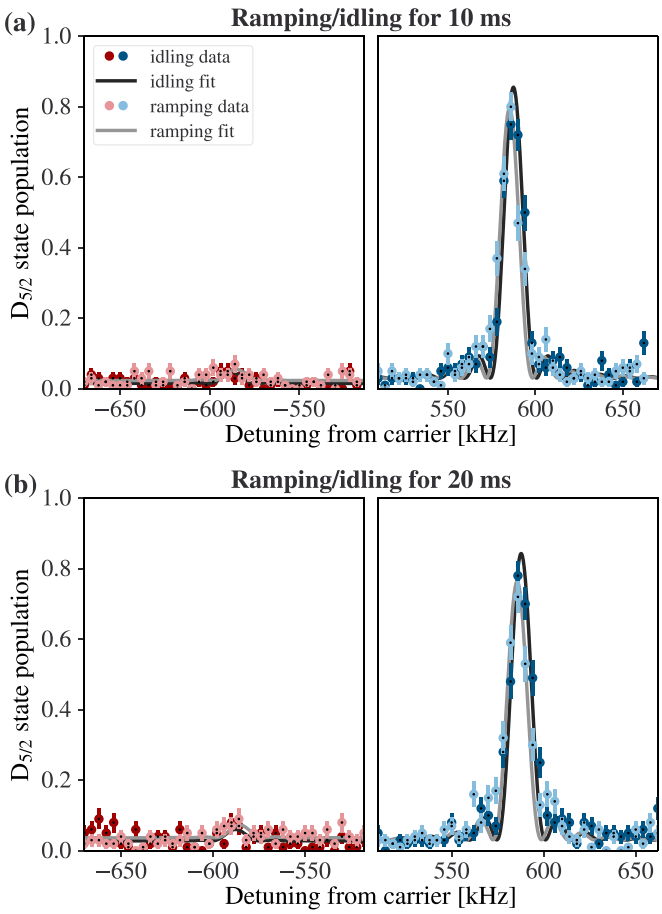


FIG. 9. Results of measuring the amount of ion heating induced by adiabatic ramping over (a) 10 ms and (b) 20 ms plotted with a control experiment in which the ion is allowed to idle for the same amount of time. Here, the light points (both red and blue) represent the adiabatic ramping experiments with these data fit to a light gray line while the dark points and the black line represent the control experiments.

ramping is 0.08(2) compared to 0.05(2) when idling for the same amount of time. For $T_r = 20$ ms, the phonon number after ramping is 0.12(2) compared to 0.07(5). For ramping time $T_r = 20$ ms, the ramping speed is $2\pi \times 20$ kHz/ms and the fidelity loss in a linear ramping process is calculated to be 3.5% according to the Landau-Zener equation [22]. Both results demonstrate the potential for faster sweeping without exciting the phonon mode, which will be used to implement faster and nonlinear sweeping in future searches of the dipole-phonon interaction.

Our current experimental results show a low-heating rate and suggest the signal-to-noise ratio will be high enough to measure the DPQL signature. Besides the test of adiabatic motional state control, we do not expect to see the DPQL signal due to the perpendicular alignment of the magnetic field to the trap axis in our current setup. This alignment results in the electric field due to the ion motion coupling molecular states with $\Delta m = \pm 1$. The energy difference between these states is dominated by the Zeeman shift, which is expected to be $2\pi \times 2$ MHz/G [22] and will be $\sim 2\pi \times 12$ MHz for our experiment, falling outside the range of frequencies covered by our current ramping experiments. However, by changing the orientation of the magnetic field along the trap axis, we can bring the energy difference within the ramping range.

## V. CONCLUSION

We have demonstrated the sympathetic cooling of the axial modes of a $Ca^+$-$CaO^+$ ion chain to near the ground state of motion via pulsed sideband cooling on the cotrapped $Ca^+$ ion. We have also shown the ramping of the out-of-phase mode frequency over the predicted ground rotational state $\Lambda$-doublet frequency splitting at a rate compatible with adiabatic state transfer. We find that the ramping leads to a minimal increase in phonon number, which we attribute to ion heating. This background rate is compatible with starting a search for the DPQL signal.

Two additional steps are required to observe the DPQL signal. The first step is to change the magnetic field orientation to be parallel with the trap axis such that the dipole-phonon interactions drive $\Delta m = 0$ transitions. The second step is the preparation of the molecule into the ground state. One method is to use DPQL to project into the desired state. At room temperature, we expect that the ground rotational state population is only 0.5%. Although its population is low, the ground state has a black-body limited lifetime of 4 s [22]. The lifetime will enable us to perform hundreds of experimental trials after an initial detection before the state changes. An alternate approach would be to set up the experiment in a cryogenic environment.

## ACKNOWLEDGMENTS

We thank Wes Campbell and Eric Hudson for helpful discussions. This work is supported by the Army Research Office (Grant No. W911NF-21-1-0346). Support is also acknowledged from the U.S. Department of Energy, Office of Science, National Quantum Information Science Research Centers, Quantum Systems Accelerator.

[1] O. O. Versolato, M. Schwarz, A. K. Hansen, A. D. Gingell, A. Windberger, J. Ullrich, F. Jensen, J. R. Crespo López-Urrutia, and M. Drewsen, Decay Rate Measurement of the First Vibrationally Excited State of $MgH^+$ in a Cryogenic Paul Trap, Phys. Rev. Lett. **111**, 053002 (2013).

[2] C. W. Chou, A. L. Collopy, C. Kurz, Y. Lin, M. E. Harding, P. N. Plessow, T. Fortier, S. Diddams, D. Leibfried, and D. R. Leibrandt, Frequency-comb spectroscopy on pure quantum states of a single molecular ion, Science **367**, 1458 (2020).

[3] S. Schiller and V. Korobov, Tests of time independence of the electron and nuclear masses with ultracold molecules, Phys. Rev. A **71**, 032505 (2005).

[4] V. V. Flambaum and M. G. Kozlov, Enhanced Sensitivity to the Time Variation of the Fine-Structure Constant and $m_p/m_e$ in Diatomic Molecules, Phys. Rev. Lett. **99**, 150801 (2007).

[5] M. Kajita, M. Abe, M. Hada, and Y. Moriwaki, Proposed detection of variation in $m_p/m_e$ using a vibrational transition frequency of $aCaH^+$ ion estimated accuracies of pure $XH^+$(X: even isotopes of group II atoms) vibrational transition frequencies: towards the test of the variance in $m_p/m_e$, J. Phys. B: At. Mol. Opt. Phys **44**, 209802 (2011).

[6] S. Alighanbari, M. G. Hansen, V. I. Korobov, and S. Schiller, Rotational spectroscopy of cold and trapped molecular ions in the Lamb–Dicke regime, Nat. Phys. **14**, 555 (2018).

[7] I. Kortunov, S. Alighanbari, M. Hansen, G. Giri, V. Korobov, and S. Schiller, Proton–electron mass ratio by high-resolution optical spectroscopy of ion ensembles in the resolved-carrier regime, Nat. Phys. **17**, 569 (2021).

[8] E. R. Meyer, J. L. Bohn, and M. P. Deskevich, Candidate molecular ions for an electron electric dipole moment experiment, Phys. Rev. A **73**, 062108 (2006).

[9] A. N. Petrov, N. S. Mosyagin, T. A. Isaev, and A. V. Titov, Theoretical study of $HfF^+$ in search of the electron electric dipole moment, Phys. Rev. A **76**, 030501(R) (2007).

[10] H. Loh, K. C. Cossel, M. Grau, K.-K. Ni, E. R. Meyer, J. L. Bohn, J. Ye, and E. A. Cornell, Precision spectroscopy of polarized molecules in an ion trap, Science **342**, 1220 (2013).

[11] S. Willitsch, Coulomb-crystallised molecular ions in traps: Methods, applications, prospects, Int. Rev. Phys. Chem. **31**, 175 (2012).

[12] A. T. Calvin and K. R. Brown, Spectroscopy of molecular ions in Coulomb crystals, J. Phys. Chem. Lett. **9**, 5797 (2018).

[13] J. Toscano, H. J. Lewandowski, and B. R. Heazlewood, Cold and controlled chemical reaction dynamics, Phys. Chem. Chem. Phys. **22**, 9180 (2020).

[14] R. Rugango, J. E. Goeders, T. H. Dixon, J. M. Gray, N. Khanyile, G. Shu, R. J. Clark, and K. R. Brown, Sympathetic cooling of molecular ion motion to the ground state, New J. Phys. **17**, 035009 (2015).

[15] Y. Wan, F. Gebert, F. Wolf, and P. O. Schmidt, Efficient sympathetic motional-ground-state cooling of a molecular ion, Phys. Rev. A **91**, 043425 (2015).

[16] F. Wolf, Y. Wan, J. C. Heip, F. Gebert, C. Shi, and P. O. Schmidt, Non-destructive state detection for quantum logic spectroscopy of molecular ions, Nature (London) **530**, 457 (2016).

[17] C.-w. Chou, C. Kurz, D. B. Hume, P. N. Plessow, D. R. Leibrandt, and D. Leibfried, Preparation and coherent manipulation of pure quantum states of a single molecular ion, Nature (London) **545**, 203 (2017).

[18] M. Sinhal, Z. Meir, K. Najafian, G. Hegi, and S. Willitsch, Quantum-nondemolition state detection and spectroscopy of single trapped molecules, Science **367**, 1213 (2020).

[19] G. Poulsen, Sideband cooling of atomic and molecular ions, Ph.D. thesis, University of Aarhus, 2011.

[20] D. Kielpinski, B. E. King, C. J. Myatt, C. A. Sackett, Q. A. Turchette, W. M. Itano, C. Monroe, D. J. Wineland, and W. H. Zurek, Sympathetic cooling of trapped ions for quantum logic, Phys. Rev. A **61**, 032310 (2000).

[21] W. C. Campbell and E. R. Hudson, Dipole-Phonon Quantum Logic with Trapped Polar Molecular Ions, Phys. Rev. Lett. **125**, 120501 (2020).

[22] M. Mills, H. Wu, E. C. Reed, L. Qi, K. R. Brown, C. Schneider, M. C. Heaven, W. C. Campbell, and E. R. Hudson, Dipole–phonon quantum logic with alkaline-earth monoxide and monosulfide cations, Phys. Chem. Chem. Phys. **22**, 24964 (2020).

[23] J. E. Goeders, C. R. Clark, G. Vittorini, K. Wright, C. R. Viteri, and K. R. Brown, Identifying single molecular ions by resolved sideband measurements, J. Phys. Chem. A **117**, 9725 (2013).

[24] H.-K. Lau and D. F. V. James, Proposal for a scalable universal bosonic simulator using individually trapped ions, Phys. Rev. A **85**, 062329 (2012).

[25] M. Palmero, R. Bowler, J. P. Gaebler, D. Leibfried, and J. G. Muga, Fast transport of mixed-species ion chains within a Paul trap, Phys. Rev. A **90**, 053408 (2014).

[26] R. B. Blakestad, C. Ospelkaus, A. P. VanDevender, J. M. Amini, J. Britton, D. Leibfried, and D. J. Wineland, High-Fidelity Transport of Trapped-Ion Qubits through an **X**-Junction Trap Array, Phys. Rev. Lett. **102**, 153002 (2009).

[27] R. B. Blakestad, C. Ospelkaus, A. P. VanDevender, J. H. Wesenberg, M. J. Biercuk, D. Leibfried, and D. J. Wineland, Near-ground-state transport of trapped-ion qubits through a multidimensional array, Phys. Rev. A **84**, 032314 (2011).

[28] V. Kaushal, B. Lekitsch, A. Stahl, J. Hilder, D. Pijn, C. Schmiegelow, A. Bermudez, M. Müller, F. Schmidt-Kaler, and U. Poschinger, Shuttling-based trapped-ion quantum information processing, AVS Quantum Sci. **2**, 014101 (2020).

[29] G. Poulsen and M. Drewsen, Adiabatic cooling of a single trapped ion, arXiv:1210.4309.

[30] F. Karin, Adiabatic cooling for rovibrational spectroscopy of molecular ions, Ph.D. thesis, University of Aarhus, 2017.

[31] S. Willitsch, M. T. Bell, A. D. Gingell, and T. P. Softley, Chemical applications of laser- and sympathetically-cooled ions in ion traps, Phys. Chem. Chem. Phys. **10**, 7200 (2008).

[32] Z. Meir, T. Sikorsky, R. Ben-shlomi, N. Akerman, Y. Dallal, and R. Ozeri, Dynamics of a Ground-State Cooled Ion Colliding with Ultracold Atoms, Phys. Rev. Lett. **117**, 243401 (2016).

[33] J. B. Wübbena, S. Amairi, O. Mandel, and P. O. Schmidt, Sympathetic cooling of mixed-species two-ion crystals for precision spectroscopy, Phys. Rev. A **85**, 043412 (2012).

[34] Q. A. Turchette, D. Kielpinski, B. E. King, D. Leibfried, D. M. Meekhof, C. J. Myatt, M. A. Rowe, C. A. Sackett, C. S. Wood, W. M. Itano, C. Monroe, and D. J. Wineland, Heating of trapped ions from the quantum ground state, Phys. Rev. A **61**, 063418 (2000).

[35] C. Marquet, F. Schmidt-Kaler, and D. F. James, Phonon–phonon interactions due to non-linear effects in a linear ion trap, Appl. Phys. B **76**, 199 (2003).

[36] C. Zener, Non-adiabatic crossing of energy levels, Proc. R. Soc. London, Ser. A **137**, 696 (1932).

[37] S. Wolf, Ion crystals for fundamental research on matter-antimatter symmetry and on photon statistics, Ph.D. thesis, Johannes Gutenberg University Mainz, 2019.

[38] S. Bourdeauducq, R. Jördens, P. Zotov, J. Britton, D. Slichter, D. Leibrandt, D. Allcock, A. Hankin, F. Kermarrec, Y. Sionneau, R. Srinivas, T. R. Tan, and J. Bohnet, ARTIQ 1.0, Zenodo (2016), doi: 10.5281/zenodo.51303.

[39] G. Kasprowicz, P. Kulik, M. Gaska, T. Przywozki, K. Pozniak, J. Jarosinski, J. W. Britton, T. Harty, C. Balance, W. Zhang, D. Nadlinger, D. Slichter, D. Allcock, S. Bourdeauducq, R. Jördens, and K. Pozniak, ARTIQ and SINARA: Open software and hardware stacks for quantum physics, *OSA Quantum 2.0 Conference* (Optical Society of America, Washington, DC, 2020), p. QTu8B.14.

[40] L. Riesebos, B. Bondurant, J. Whitlow, J. Kim, M. Kuzyk, T. Chen, S. Phiri, Y. Wang, C. Fang, A. Van Horn *et al.*, Modular software for real-time quantum control systems, in *2022 IEEE International Conference on Quantum Computing and Engineering* (IEEE, New York, 2022).

[41] L. Riesebos, B. Bondurant, and K. Brown, Duke ARTIQ extensions (DAX) (2021), https://gitlab.com/duke-artiq/dax.

[42] T. B. T. Baba and I. W. I. Waki, Cooling and mass-analysis of molecules using laser-cooled atoms, Jpn. J. Appl. Phys. **35**, L1134 (1996).

[43] A. Walther, F. Ziesel, T. Ruster, S. T. Dawkins, K. Ott, M. Hettrich, K. Singer, F. Schmidt-Kaler, and U. Poschinger, Controlling Fast Transport of Cold Trapped Ions, Phys. Rev. Lett. **109**, 080501 (2012).